

PCCP

Accepted Manuscript



This article can be cited before page numbers have been issued, to do this please use: C. Noh and Y. Jung, *Phys. Chem. Chem. Phys.*, 2019, DOI: 10.1039/C8CP07200K.



This is an Accepted Manuscript, which has been through the Royal Society of Chemistry peer review process and has been accepted for publication.

Accepted Manuscripts are published online shortly after acceptance, before technical editing, formatting and proof reading. Using this free service, authors can make their results available to the community, in citable form, before we publish the edited article. We will replace this Accepted Manuscript with the edited and formatted Advance Article as soon as it is available.

You can find more information about Accepted Manuscripts in the [author guidelines](#).

Please note that technical editing may introduce minor changes to the text and/or graphics, which may alter content. The journal's standard [Terms & Conditions](#) and the ethical guidelines, outlined in our [author and reviewer resource centre](#), still apply. In no event shall the Royal Society of Chemistry be held responsible for any errors or omissions in this Accepted Manuscript or any consequences arising from the use of any information it contains.

Journal Name

ARTICLE TYPE

Cite this: DOI: 10.1039/xxxxxxxxxx

Understanding the Charging Dynamics of the Ionic Liquid Electric Double Layer Capacitor via Molecular Dynamics Simulations

Chanwoo Noh and YounJoon Jung*

Received Date

Accepted Date

DOI: 10.1039/xxxxxxxxxx

www.rsc.org/journalname

We investigate the charging phenomena of the electric double layer capacitor (EDLC) by conducting both the equilibrium and non-equilibrium molecular dynamics (MD) simulations. Graphene electrode and 1-ethyl-3-methylimidazolium thiocyanate ($[\text{EMIM}]^+[\text{SCN}]^-$) ionic liquid were used as a system for the EDLC. We clarify the ionic layer structure and show that an abrupt change of the ionic layers leads to a high differential capacitance of EDLC. The charging simulations reveal that the charging dynamics of the EDLC is highly dependent on the rearrangement of the ionic layer structure. Particularly, the electrode charge during the charging process is consistent with the perpendicular displacement of ionic liquid molecules. From this property, we analyze the contribution of each molecular ion to the electrode charge stored during charging. Charging of the EDLC is largely dependent on the desorption of the co-ions from the electrode rather than the adsorption of the counter-ions. In addition, the contribution of bulk ions to the charge stored in the EDLC is as important as that of ions adjacent to the electrode surface contrary to the conventional viewpoint. From these results, we identify the charging mechanism of the EDLC and discuss the relevance to experimental results. Our findings in the present study are expected to play an important role in designing an efficient EDLC with a novel perspective on the charging of the EDLC.

1 Introduction

An electric double layer capacitor (EDLC), or a supercapacitor, is a promising energy storage device with a superb power density and a good energy density.^{1,2} Its superior electrical performance arises from the electric double layer (EDL), which is a layer structure formed by adsorbing electrolyte ions with opposite charges on a charged electrode.^{3–10} Ions can quickly rearrange themselves in such a way that the electric field generated by the electrode charge can be screened within a subnanometer length scale. In addition, since the EDL structure is not accompanied by any chemical reaction, EDLC has a higher cyclability and a faster charging rate than conventional chemical cells.

In particular, EDLCs using carbon nano-material as an electrode show excellent performance.^{11–14} Carbon nano-electrodes maximize the electrode surface area in EDLCs to improve capacity and energy density.^{15,16} Among various carbon-nanomaterials, graphene-based materials are promising candidates for replacing conventional EDLC electrodes. Graphene has remarkable advan-

tages such as a large surface area, a high electrical conductivity, a great mechanical stiffness, and an efficient electrolyte adsorption property.^{17,18} In particular, it serves as a prototype for EDLC due to its simple, flat structure. Due to these properties, EDLCs consisting of graphene have been studied in many experiments and computer simulations,^{3,11,19–24} and they have shown superior performances compared to conventional capacitors.

In addition to the electrodes, electrolytes also play an important role in determining the performance of the EDLCs. The energy density and the power density of the EDLC are proportional to the square of the operating potential, so increasing the operating potential of the EDLC is important for achieving a high energy and power density of the EDLCs.¹ Generally, the maximum operating potential is limited by the electrochemical window of the electrolytes. Aqueous electrolytes, which are commonly used in the EDLC, have the disadvantage of narrow electrochemical windows within 2 V. To overcome this problem, ionic liquids have been used as an alternative electrolytes in the EDLCs.^{25–28} Ionic liquids have advantages of a wide electrochemical windows up to 4–5 V, a low volatility, and a high boiling temperature, so the EDLC can operate in more severe conditions.²⁹ However, ionic liquids have some drawbacks as well as the aforementioned advantages as the electrolytes of the EDLCs. The conductivities

Department of Chemistry, Seoul National University, Seoul 08826, Korea Fax: (+82) 2-880-4369; Tel: (+82) 2-880-4369; E-mail: yjung@snu.ac.kr

† Electronic Supplementary Information (ESI) available. See DOI: 10.1039/b000000x/

of ionic liquids are lower than conventional electrolytes due to their high viscosity, which may result in a reduced power density. Therefore, it is very important and necessary to understand the dynamical properties of the electric double layer of ionic liquids in order to design EDLCs with desirable properties.

Fundamental theories for EDLs have been developed along with the application of the EDLC. The most basic theory of the EDL is the Helmholtz theory, which describes the EDL as a simple monolayer of counter-ions adsorbed on the electrode. In this theory, however, any space charge of ions behind the first ion layer is not considered.³⁰ To overcome this limitation, the Gouy-Chapman theory describes the EDL as a diffuse layer with a constant thickness, taking into account thermal fluctuation effects. While being a simple model, the Gouy-Chapman theory can explain the behavior of the EDL of the dilute electrolyte successfully.³¹ However, EDLs with a high ion density cannot be described by these simple theories. Recently developed theories based on the Landau-Ginzburg model or the mean-field theory have been successful in explaining the structural aspect of the EDL of ionic liquids.^{14,32-34} The ionic liquid EDL described in these theories exhibits an oscillating structure from the electrode due to the *crowding* and *overscreening* effects.

Based on the theoretical development of the EDL of the ionic liquids, its structure has been discovered in various experiments and computational simulations. The ionic density and the thicknesses of ionic layers have been characterized by *in situ* NMR,³⁵ X-ray spectroscopy,^{36,37} and the AFM experiments.^{38,39} These experiments revealed that the counter-ions directly contact with the electrode, and the EDL of ionic liquids consists of alternating layers of anions and cations. Combining with the molecular examination of molecular dynamics (MD) simulation studies,⁴⁰⁻⁴⁴ there have been significant advances in understanding the complex structure of ionic layers in the EDLC. However, most of these studies have focused on the static equilibrium properties of the EDLC, which did not directly examine the process of charging. Although there are several MD simulation studies of charging,⁴⁵⁻⁴⁸ in-depth analysis of the ionic layer structure is still desirable. The dynamics of the EDL is directly related to the time-dependent properties in EDLCs, such as power density and the charging/discharging rate. In addition, recent studies have shown that the capacitance of the EDLC is highly correlated with the ionic layer structure of the electrolyte, even 10 Å far away from the electrodes.^{21,22} Thus, it is necessary to investigate the evolution of the EDL during the charging and discharging in order to fully understand the behavior of the EDLC.

In this paper, we investigated the charging and discharging dynamics of the EDLC with ionic liquids by conducting the non-equilibrium MD simulations under the constant potential condition. We analyzed the motion of ions during the charging process and confirmed the relationship between the charging dynamics and the ionic layer structures. The current work is based on our previous study,²² where we investigated the charging mechanism of the cyano-based ionic liquids EDLC and its molecular origin. In this work, we focused on 1-ethyl-3-methyl imidazolium thiocyanate ($[\text{EMIM}]^+[\text{SCN}]^-$), the electrolyte which exhibits the largest capacitance among cyano-based ionic liquids studied in

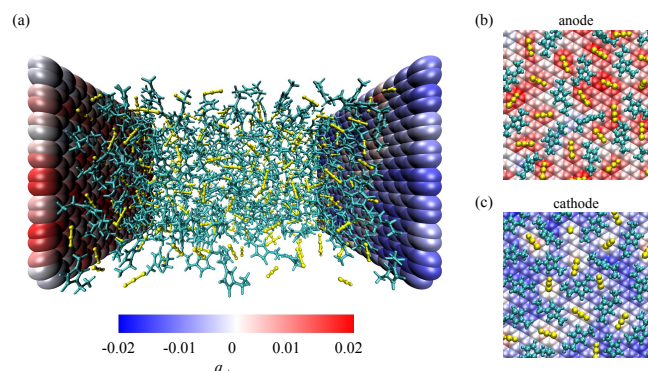


Fig. 1 Representative snapshots of our simulation at $\Delta\Psi = 2$ V. The charge of each electrode atom is indicated by its color, which is referred to color scale bar (unit e). Here, the left electrode is the anode, and the right one is the cathode. Between these electrodes, pure $[\text{EMIM}]^+$ and $[\text{SCN}]^-$ ions are filled as an electrolyte. $[\text{EMIM}]^+$ and $[\text{SCN}]^-$ ions are depicted as cyan and yellow molecular ions, respectively. The distance between the two electrodes is fixed as 6 nm.

our previous work. It is known that $[\text{EMIM}]^+[\text{SCN}]^-$ has a sufficiently wide electrochemical window of 3.2 V,⁴⁹ and it has the advantages of higher conductivity and lower viscosity at room temperature than more commonly used ionic liquids, such as $[\text{EMIM}]^+[\text{BF}_4]^-$ and $[\text{BMIM}]^+[\text{PF}_6]^-$.²⁸

The rest of the paper is organized as follows. Section 2 presents the brief description of the system and the MD method used in this study. In Section 3, electric double layer structure, differential capacitance, and the charging dynamics of the EDLC are analyzed. Conclusions are given in Section 4.

2 Models and Methods

In our simulation system, two parallel graphene walls were used as the electrodes, and the $[\text{EMIM}]^+[\text{SCN}]^-$ ionic liquid confined between them was used as an electrolyte (Fig. 1). A total of 256 ion pairs are used as electrolyte molecules, and each electrode consists of 448 carbon atoms with the dimension of $33.96 \times 34.31 \text{ \AA}^2$. The distance between the two electrodes is fixed as 60 Å, which is wide enough that the middle part of the system forms a bulk phase. The system size was determined via *NPT* MD simulation of the pure $[\text{EMIM}]^+[\text{SCN}]^-$ liquids. Ions were modeled with flexible OPLS all-atom force fields. Parameters of the $[\text{EMIM}]^+$ cation were taken from the study on the imidazolium-based ionic liquids,^{50,51} and the $[\text{SCN}]^-$ anion parameters were taken from a previous study of cyano-anion ionic liquids.⁵² Exact parameters are compiled in the supporting information of the references reported by Canongia Lopes *et al.*⁵⁰ and Dhungana *et al.*⁵². Graphene atoms were described as fixed Lennard-Jones particles with a diameter of $\sigma_{\text{LJ}} = 3.4 \text{ \AA}$ and a depth of the potential well of $\epsilon_{\text{LJ}} = 0.086 \text{ kcal/mole}$.⁵³ Force-field parameters between different atomic species were evaluated from the Lorentz-Berthelot rules.

All our MD simulations were performed using LAMMPS program.⁵⁴ The motion of particles was integrated using the velocity Verlet algorithm with 1 fs timestep. The cutoff distances for non-bonded interactions were set to 1.4 nm. Systems were equili-

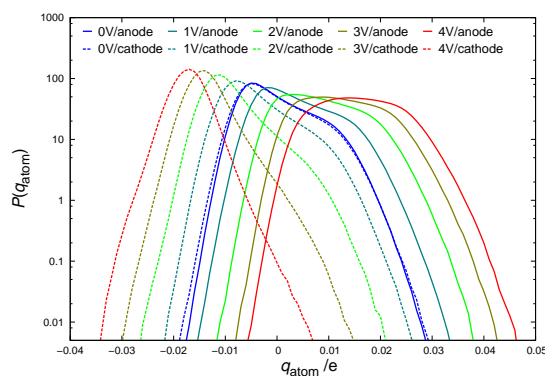


Fig. 2 Distribution of electrode atom charges at the various electrostatic potential difference between the anode and the cathode, $\Delta\Psi$. The legend key is expressed as the form of “ $\Delta\Psi$ /electrode”. Solid and dashed lines denote the distributions for the anode and the cathode, respectively.

brated for longer than 10 ns using simulated annealing from 800 K to 350 K, and production runs were conducted at 350 K. The temperature was controlled using Nosé-Hoover thermostat with a relaxation time of 100 fs during the *NVT* simulations. A constant potential method (CPM)⁵⁵ was applied to control the electrostatic potential between two electrodes. In this method, the charges of the electrode atoms are described as a Gaussian function, and they are allowed to fluctuate during simulations to maintain the constant potential difference between the electrodes. The Gaussian function parameter for the graphene electrode is set to 19.79 nm⁻¹, which is the same as that of a three-layer graphite.⁵⁶ The charges of the electrolyte ion atoms are described as a fixed point charge. The CPM was conducted with the *comp* module implemented in the LAMMPS.⁵⁶ In this module, 3D-periodic Ewald summation with shape corrections⁵⁷ was applied to describe the slab geometry of the system, and the particle-particle particle-mesh (PPPM) method was used to evaluate the Coulombic interactions.⁵⁸

3 Results and Discussions

3.1 Electrode charge fluctuation

We first validated our constant potential simulations on the graphene-[EMIM]⁺[SCN]⁻ EDLC system. In our simulations, the electrostatic potential at the anode is higher than that of the cathode by $\Delta\Psi$. $\Delta\Psi$ is defined as $\Delta\Psi = \Psi_{\text{anode}} - \Psi_{\text{cathode}}$, where Ψ_{anode} and Ψ_{cathode} are the electrostatic potentials applied at the anode and the cathode, respectively. The anode and the cathode are charged with positive and negative potential values, respectively. The charge of each electrode atom is not fixed as a constant value during simulation, but fluctuates depending on the local electrostatic environment and the potential bias applied in the system. As shown in Fig. 1, both [EMIM]⁺ and [SCN]⁻ ions can be adjacent to the anode and cathode surfaces depending on the local environment, and the local charge induced on the electrode turns out to be highly correlated with the adjacent interfacial ions. The correlation can be analyzed by the distribution of individual charges of the electrode atoms.

Fig. 2 shows the probability distribution of atomic charges in

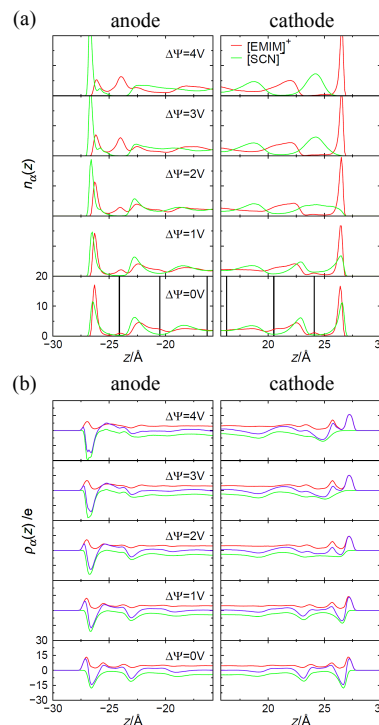


Fig. 3 (a) The number density $n_\alpha(z)$ and (b) the charge density $\rho_\alpha(z)$ of $[\text{EMIM}]^+$ and $[\text{SCN}]^-$ ions. The anode is located at $z = -30 \text{ \AA}$, and the cathode is located at $z = 30 \text{ \AA}$. The values for cations and anions are represented as red and green, respectively. Black vertical lines denote the minimum positions of $n_{[\text{SCN}]^-}(z)$ in $\Delta\Psi = 0 \text{ V}$ condition. Purple lines in the charge density $\rho_\alpha(z)$ denote the total charge density, which is defined as $\rho_{[\text{EMIM}]^+}(z) + \rho_{[\text{SCN}]^-}(z)$.

each electrode, $p(q_{\text{atom}})$, under various $\Delta\Psi$ conditions. When $\Delta\Psi = 0 \text{ V}$ is applied, $p(q_{\text{atom}})$ of two electrodes are in coincidence. However, when finite $\Delta\Psi$ is applied, the anode and the cathode are charged with opposite values, and the probability distribution for each electrode develops different characteristic behaviors. This asymmetry indicates that not only the electrodes have opposite charge values but also the environment around the two electrodes become completely different. It should be noted that the probability distribution exhibits a non-Gaussian behavior at all potential conditions, even at $\Delta\Psi = 0 \text{ V}$. For the organic electrolyte/salt-based EDLC, a non-Gaussian distribution has been observed only under high potential conditions.⁵⁶ The non-Gaussian nature in the ionic liquid EDLC is due to the high ionic density near the electrode surface and the asymmetric shape and charge distribution of the molecular ions. In addition, even when $\Delta\Psi$ is as large as up to 3 V, there always exists an atom with an opposite charge to the electrode charge due to the broad distribution of $p(q_{\text{atom}})$. Overall, it is clear that the fluctuation of the electrode charge is critical in understanding the structure of the ionic liquid EDLC, so it is necessary to utilize the CPM in studying dynamical behavior of the EDLC of our system.

3.2 Ionic layer structures

We investigated the ionic layer structure near the graphene electrodes via number density and charge density. Number density

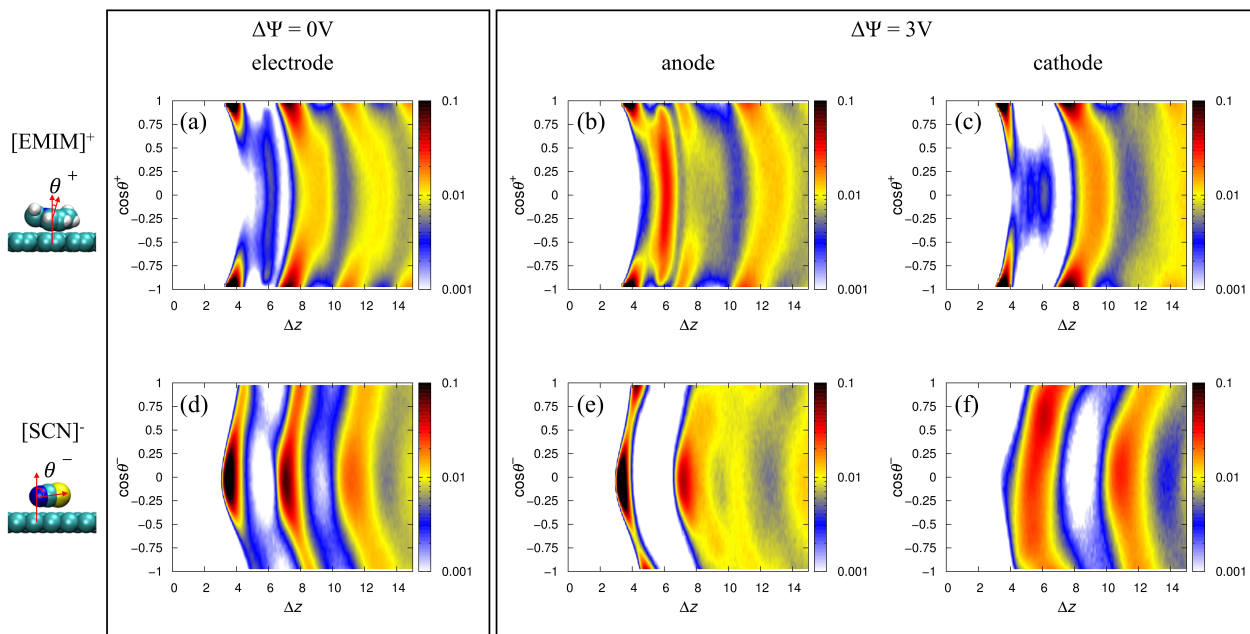


Fig. 4 The contour map of the ionic layer structures. Δz denotes the distance of the ion from the electrode, and $\cos\theta^\pm$ denotes the orientation of specific ions. The graphical description of angles θ^\pm are presented at the left panel. The probability density increases in the order of white-blue-yellow-red-black. (a), (d) The contour map of $[\text{EMIM}]^+$ and $[\text{SCN}]^-$ ions when zero electrode potential is applied. (b), (c) The contour map of $[\text{EMIM}]^+$ ions near the anode and cathode when electrode potential $\Delta\Psi = 3$ V is applied. (e), (f) The contour map of $[\text{SCN}]^-$ ions near the anode and cathode when electrode potential $\Delta\Psi = 3$ V is applied.

distribution $n_\alpha(z)$ of the specific ion α is defined as the integration of the center of mass distribution of ions $n_\alpha(x',y',z)$, expressed as following equation,

$$n_\alpha(z) = A_0^{-1} \int_{-x_0}^{x_0} \int_{-y_0}^{y_0} dx' dy' n_\alpha(x',y',z). \quad (1)$$

Here, A_0 is the electrode surface area. Similar to the number density $n_\alpha(z)$, the charge density distribution $\rho_\alpha(z)$ is defined by the following equation,

$$\rho_\alpha(z) = A_0^{-1} \int_{-x_0}^{x_0} \int_{-y_0}^{y_0} dx' dy' \rho_\alpha(x',y',z), \quad (2)$$

where $\rho_\alpha(x',y',z)$ is the local atomic charge density of the ion α .

Fig. 3 shows $n_\alpha(z)$ and $\rho_\alpha(z)$ in various $\Delta\Psi$ conditions. The anode and the cathode are located at $z = -30$ Å and $z = 30$ Å, respectively. The ions form the first ionic layer at 3.5 Å away from the electrode, which is the closest distance to the graphene surface due to the size of the particles. After the first ionic layer, the oscillating ion density along the z direction reflects the formation of additional ionic layers. This oscillating layer structure is a common feature in the ionic liquid EDLC.^{5,59–61} When there is no potential difference between the electrodes, the maximum density positions of $[\text{EMIM}]^+$ and $[\text{SCN}]^-$ overlap with each other. This is because the local electroneutrality should be satisfied and the layer thicknesses of the two ions are similar to each other. However, when the electrodes are charged due to the finite potential difference, the first ionic layer is filled with counter-ions, while co-ions are expelled from the electrode. If a potential difference greater than 3 V is applied, the alternating layers of the counter-ions and co-ions are formed. Particularly, the ionic layer

structure changes abruptly under $\Delta\Psi = 2$ V condition: the first and the second $[\text{SCN}]^-$ ion layers near the cathode merge into their intermediate position.

Charge densities of $[\text{EMIM}]^+$ and $[\text{SCN}]^-$ ions also show oscillations with respect to the z direction near the electrode surface. When we compare $\rho_\alpha(z)$ and $n_\alpha(z)$, the oscillatory behavior of the charge density almost disappears within 10 Å from the electrode, while that of the number density persists beyond that distance. This observation indicates that molecular ions efficiently rearrange themselves by maximizing the Coulomb interaction with other particles in the vicinity.^{12,41,62} Interestingly, all the charge densities from the electrodes initially show positive peaks even near the anode in $\Delta\Psi = 4$ V condition. Under the potential condition we consider, $[\text{SCN}]^-$ ions cannot fully replace the $[\text{EMIM}]^+$ ions in the first layer due to a strong $\pi-\pi$ stacking interaction between the cations and graphene electrodes. It is worth noting that the ionic layer structures of Fig. 3 are consistent with those from our previous work done under the constant charge condition,²² and the direct comparison between the two is depicted in Fig. S1. A good agreement arises because the fluctuation of the electrode charge is averaged out for the static thermodynamical properties in equilibrium. However, it does not mean that the electrode charge fluctuation is unimportant in the dynamical properties of the EDLC. To the contrary, the opposite is the case as will be shown later.

So far, we have studied the structure of the ionic layer according to the distance from the electrode surface. However, in order to better understand the ionic layer structure, not only the distance from the electrode but also the orientation of the ions must be considered simultaneously. To describe the orientation of each

ion, the angles θ^\pm are defined as follows. For $[\text{EMIM}]^+$ ions, θ^+ is defined as an angle between an electrode normal vector and an $[\text{EMIM}]^+$ ring normal vector, while θ^- of $[\text{SCN}]^-$ ions is defined as an angle between an electrode normal vector and a vector from a nitrogen atom to a sulfur atom in the $[\text{SCN}]^-$ ion. For clarity, the graphical description of θ^\pm is presented in the Fig. 4. According to these definitions, $\cos\theta^+$ and $\cos\theta^-$ are equal to 1 and 0, respectively, when the corresponding ions are parallel to the electrode.

Fig. 4 shows the probability distribution of ions with respect to $\cos\theta^\pm$ and Δz , the distance from the electrode. When no potential bias is applied, both $[\text{EMIM}]^+$ and $[\text{SCN}]^-$ ions adjacent to the graphene electrodes maintain a parallel arrangement with respect to the electrodes. The parallel arrangement of the $[\text{EMIM}]^+$ ions is due to that the $[\text{EMIM}]^+$ ions form a strong $\pi - \pi$ stacking interaction with electrodes. The $[\text{SCN}]^-$ ions also maintain a parallel arrangement with respect to the electrodes to maximize the Coulombic interaction with the parallelly aligned $[\text{EMIM}]^+$ ions. Since the thicknesses of the two ions forming the ionic layer are equal to that of a single carbon atom, the neighboring ionic layers are arranged similar to the first ionic layer. As a result, the orientation of ions is maintained as parallel until the third layer, indicating that the ionic layer is not a localized structure only next to the electrode.

When $\Delta\Psi = 3$ V is applied, ionic layers near each electrode change in distinct manners. In the vicinity of the anode, a portion of $[\text{EMIM}]^+$ ions forming $\pi - \pi$ stacking with the electrode rotate in the vertical direction and desorb from the electrode. As this pre-empted space becomes filled with $[\text{SCN}]^-$ ions coming from the second layer, the density of $[\text{SCN}]^-$ ions in the first ionic layer increases. Looking at the ionic layer near the cathode, $[\text{SCN}]^-$ ions parallel to the electrode rotate and desorb from the electrode, and vertically aligned $[\text{EMIM}]^+$ ions form $\pi - \pi$ stacking structure to the electrode. That is, the rearrangement of the ionic layer due to the polarization of the electrode is accompanied by rotational movements of the ions near the electrode. During the rearrangement of ionic liquids, not only the first and second ionic layers but also further ionic layers undergo significant structural changes.

As discussed in the behavior of the charge density, $\rho_\alpha(z)$, $[\text{EMIM}]^+$ ions, which is the co-ion of the anode, form a $\pi - \pi$ stacking structure with the anode, while $[\text{SCN}]^-$ ions are completely expelled from the cathode. This finding indicates that the structural rearrangement of bulky and heavy $[\text{EMIM}]^+$ ions is much more difficult than $[\text{SCN}]^-$. Therefore, it is further expected that the ionic layer change and corresponding energy stored in the EDLC are dominated by the rearrangement of $[\text{SCN}]^-$ ions.

3.3 Differential capacitance

Based on the ionic layer structures in the Fig. 3, the electrostatic potential profile along the z direction, $\Psi(z)$, can be calculated by integrating the Poisson equation as follows,

$$\Psi(z) = -4\pi \int_{-\infty}^z (z-z')\rho(z')dz'. \quad (3)$$

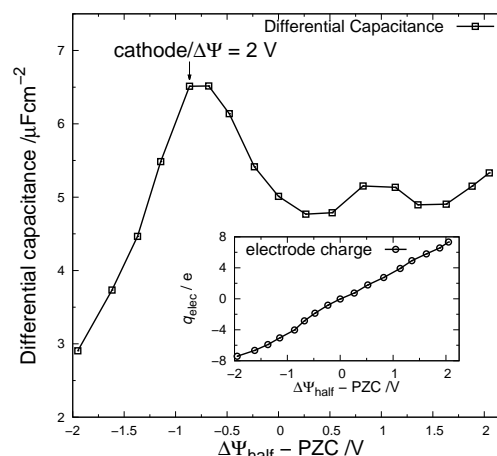


Fig. 5 Differential capacitance of the EDLC as a function of the half-cell potential. (inset) The relation between Ψ_{half} and q_{elec} .

The calculated $\Psi(z)$ in various $\Delta\Psi$ conditions are depicted in the Fig. S3 of the supplementary information. Similar to $n_\alpha(z)$ and $\rho_\alpha(z)$, $\Psi(z)$ also shows an oscillatory behavior, indicating the existence of multiple ionic layers. The electrostatic potential profile becomes nearly constant in the bulk region after a sharp decrease near the electrode. The entire EDLC can be described as a serial connection of the anode and cathode half-cells. The corresponding potential drop of each half-cell is then defined by

$$\begin{aligned}\Delta\Psi_{\text{anode}} &\equiv \Psi_{\text{anode}} - \Psi_{\text{bulk}}(z=0 \text{ Å}), \\ \Delta\Psi_{\text{cathode}} &\equiv \Psi_{\text{cathode}} - \Psi_{\text{bulk}}(z=0 \text{ Å}).\end{aligned}\quad (4)$$

As a reference point, the potential of zero charge (PZC) is defined as $\Delta\Psi_{\text{half}}$ in $\Delta\Psi = 0$ V condition. PZC is calculated as 0.20 V, and such a positive PZC indicates the large affinity of the graphene electrode for $[\text{EMIM}]^+$ ions due to the $\pi - \pi$ interaction between them.

With the definition of the half-cell, the relation between $\Delta\Psi_{\text{half}}$ and the corresponding electrode charge, q_{elec} , is depicted in the inset of Fig. 5. q_{elec} increases almost linearly with $\Delta\Psi_{\text{half}}$, and the derivative of q_{elec} with respect to $\Delta\Psi_{\text{half}}$ is related to the area-specific differential capacitance (DC) as the following equation,

$$\text{DC}(\Delta\Psi_{\text{half}}) = \frac{\partial q_{\text{elec}}}{A_0 \partial \Delta\Psi_{\text{half}}}, \quad (5)$$

where A_0 is the area of the electrode. The differential capacitances were evaluated via the analytical derivative of the parabola fit of q_{elec} vs. $\Delta\Psi_{\text{half}}$ plot.²¹ Corresponding DC of the $[\text{EMIM}]^+[\text{SCN}]^-$ -EDLC shows a camel-like distribution, exhibiting a minimum near the PZC and maximum at higher potential. The maximum of the DC occurs at $\Delta\Psi_{\text{half}} = \text{PZC} - 0.865$ V, which corresponds to the cathode at $\Delta\Psi = 2$ V condition. Interestingly, the first layer of $[\text{SCN}]^-$ ion near the cathode is also entirely expelled from the electrode at the $\Delta\Psi = 2$ V condition, as depicted in the Fig. 3. This may be called a *vacating* effect, in which the desorption of co-ions from the electrode mainly contributes to the capacitance of the EDLC. The vacating effect has also been ob-

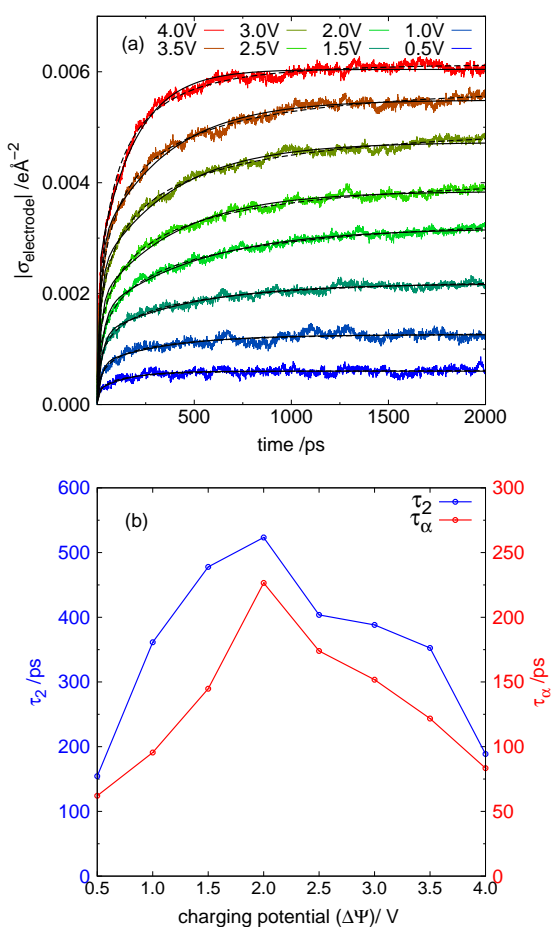


Fig. 6 (a) The charge of the electrode relaxations as a function of time when finite potentials are applied to the equilibrium states of $\Delta\Psi = 0$ V. Black solid and dashed lines are fitted curves with bi-exponential and stretched exponential functions, respectively. (b) The charging time of the EDLC as a function of $\Delta\Psi$. Blue and red lines respectively denote the τ_2 from bi-exponential fitting and τ_α from stretched exponential fitting. Here, the τ_α axis is displayed at one-half scale of the τ_2 axis.

served in other EDLC systems based on graphene oxide.^{3,63} The most important factor for inducing the vacating effect is the high ion density near the electrode. Therefore, the vacating effect is expected to be common in EDLCs with ionic liquids electrolytes and planar electrodes, and indicates that the performance of the EDLC is closely related to the rearrangement of the ionic layer.

3.4 Charging dynamics

In order to investigate the charging dynamics of the EDLC, we conduct the non-equilibrium MD simulation by applying the constant potential differences $\Delta\Psi$ between equilibrium electrodes of $\Delta\Psi = 0$ V. Firstly, the influence of the applied potential difference $\Delta\Psi$ on the charging dynamics is examined. For each condition, at least five independent trajectories are averaged out in order to reduce the statistical noise. Fig. 6 (a) shows the evolution of the charge density of electrodes $\sigma (= q_{\text{electrode}}/A_0)$ during charging. Under all conditions, most of the charging process is finished within a few hundred picoseconds, followed by an additional slow

Table 1 Relaxation times and stretching exponents of the charging dynamics

| $\Delta\Psi/V$ | τ_1/ps | τ_2/ps | τ_α/ps | β |
|----------------|--------------------|--------------------|-------------------------|---------|
| 0.5 | 3.39 | 154.46 | 62.10 | 0.489 |
| 1.0 | 20.88 | 361.41 | 95.52 | 0.435 |
| 1.5 | 24.38 | 477.85 | 144.79 | 0.397 |
| 2.0 | 26.27 | 523.29 | 226.53 | 0.403 |
| 2.5 | 17.43 | 403.67 | 173.95 | 0.429 |
| 3.0 | 16.63 | 388.14 | 151.25 | 0.419 |
| 3.5 | 16.95 | 352.60 | 121.72 | 0.437 |
| 4.0 | 6.98 | 188.79 | 83.41 | 0.533 |

charging dynamics.

To quantitatively analyze the charging dynamics, we tried to fit the evolution of electrode charge density by a single exponential function without any success, as shown in Fig. S4 of the supplementary information. This deficiency occurs because the capacitance of the supercapacitor is not constant during charging process, whose dynamics is influenced by the dynamic heterogeneity of ionic liquids.^{64–66} Thus, two kinds of relaxation functions, which have been used for dynamically heterogeneous systems, are applied, (1) bi-exponential and (2) stretched exponential functions. They are given by the following equations,

$$\sigma(t) = \sigma_{t=\infty}[1 - c \exp(-t/\tau_1) - (1-c)\exp(-t/\tau_2)], \quad (6)$$

where c , τ_1 , τ_2 , and $\sigma_{t=\infty}$ are fitting parameters, and

$$\sigma(t) = \sigma_{t=\infty}[1 - \exp(-(t/\tau_\alpha)^\beta)], \quad (7)$$

where τ_α , β , and $\sigma_{t=\infty}$ are another fitting parameters. Both fitting functions show good agreements with the simulation results. The relaxation timescales τ_1 , τ_2 , and τ_α and the stretching exponent β are tabulated in Table 1.

In most cases, τ_2 is about 20 times of τ_1 , which means that the motions with large differences in time scale coexist in the system. In addition, β has a value of 0.40 to 0.54, indicating that the charging dynamics is far from a single exponential relaxation process. These properties, as expected, indicate that the charging dynamics of the EDLC follows heterogeneous dynamics. In addition, the relaxation time exhibits an interesting non-monotonous behavior which shows a maximum value when the applied potential $\Delta\Psi$ is 2 V. As discussed above for the number density of ions $n_\alpha(z)$, the greatest transition in the ionic layer structure occurs at $\Delta\Psi \sim 2$ V condition as $[\text{SCN}]^-$ ions in the first layer adjacent to the cathode are expelled from the surface. It is not a coincidence that the ionic layer changes abruptly under the potential condition and shows the slowest charging dynamics. The charge of the electrode is proportional to the applied potential, while the layer structure changes abruptly under $\Delta\Psi \sim 2$ V condition and is almost constant thereafter. This observation means that the charging dynamics of the EDLC is highly correlated with the rearrangement of the ionic layer structure. From this correlation between the charging dynamics and the ionic layer structure, we can determine the conditions under which the ionic layer undergoes an abrupt structural rearrangement in the EDLC by measuring the

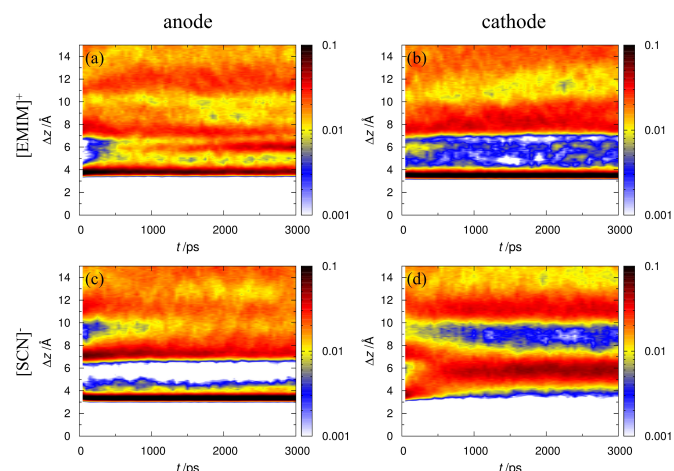


Fig. 7 Evolution of the number density of ions, $n_\alpha(\Delta z)$ as a function of time when $\Delta\Psi = 3$ V is applied. The probability density increases in the order of white-blue-yellow-red-black. Each panel represents the density of $[EMIM]^+$ ions near (a) the anode and (b) the cathode, and $[SCN]^-$ ions near (c) the anode and (d) the cathode.

charging time of the EDLC.

The evolution of the ionic layer structure during the charging of the EDLC is depicted in Fig. 7. The figure represents the $n_\alpha(\Delta z)$ as a function of time when constant $\Delta\Psi = 3$ V is applied to the unbiased equilibrium state. The ionic layers continuously change from layer structure of 0 V to that at the 3 V. In all cases, except for $[SCN]^-$ ions near the cathode, the first ionic layers located at $\Delta z = 3.5 \text{ \AA}$ are maintained during charging. Only $[SCN]^-$ ions adjacent to the cathode are completely expelled from the electrode. The ionic layer structure of the counter-ions is almost constant during the 3 ns simulations, but the co-ion layer structure evidently changes during the charging, especially in $[SCN]^-$ ions near the cathode.

As mentioned in Section 3.3, the vacating effect is commonly observed in ionic liquid EDLCs. The charging behavior for the EDLC with another ionic liquid, for example, $[EMIM]^+ [BF_4]^-$, turns out to be similar to our system as shown in the supplementary information. A vacating effect and the non-monotonic behavior in the charging time are also observed in the $[EMIM]^+ [BF_4]^-$ –EDLC, as depicted in Fig. S7 and S8 of the supplementary information. The influence of the detailed structure of the ionic liquid species is less significant on the charging dynamics than the density of ions.

As mentioned before, the relaxation of the ionic layer structure cannot be described by a single time scale. The density of the interfacial ions relaxes within a very short time, but the structure of the overall ionic layer relaxes for more than 1 ns, which is consistent with the fact that the charge of the electrode is charged on multiple time scales as depicted in Fig. 6. The multiple time scale motions in charging of the EDLC was also reported in the time-resolved X-ray experiment.⁶⁷ In their experimental study, the authors found that the time scale of the reorientation of interfacial ions was one order of magnitude larger than the time scale of the diffusion-limited ion transport, which is consistent with our

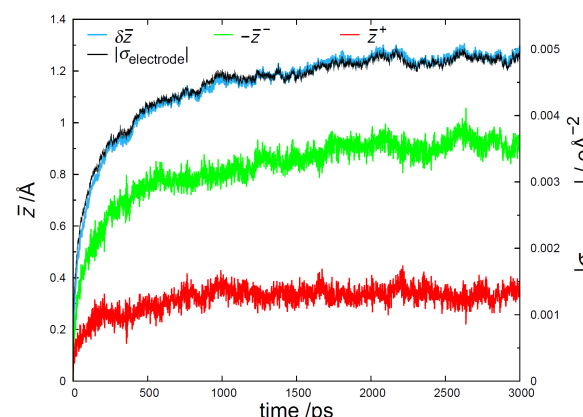


Fig. 8 Evolution of the center of mass of ions and charge of the anode when electrode is charged with $\Delta\Psi = 3$ V. Blue, green, and red lines represent $\delta\bar{z}$, $-\bar{z}^-$, and \bar{z}^+ , respectively. The black line represents the electrode charge density, $|\sigma_{\text{electrode}}|$.

findings. From the evolution of the ionic layer structure, it is suggested that the charging process of the EDLC occurs via multiple time scales. When the electrode is charged, the interfacial ions respond sensitively to the electrode charge through a diffusion within the existing ionic layer. However, if the increased electrode charge cannot be screened by the diffusive motion of ions within the first ionic layer, the electrode charge is screened by rearranging the overall ionic layer structure. The ionic layer rearrangement proceeds over a larger time scale than the diffusive motion of ions within the layer, and such a multi-stepwise motion of ions results in a heterogeneous charging dynamics.

So far, it has been confirmed that the charging of the EDLC is greatly influenced by the ionic layer structure transitions. To analyze the correlation between electrode charge and ionic layer structure quantitatively, we calculate the average perpendicular displacement of α ions with respect to the electrode, \bar{z}^α , defined by

$$\bar{z}^\alpha(\Delta t) = \frac{1}{N^\alpha} \sum_{i=1}^{N^\alpha} [z_i^\alpha(t = \Delta t) - z_i^\alpha(t = 0)], \quad (8)$$

$$\delta\bar{z} = \bar{z}^+ - \bar{z}^-,$$

where N^α is the number of α ions, and $z_i^\alpha(t)$ is the z component of the i th α ion position at time t . Fig. 8 shows that the evolution of the electrode charge is consistent with $\delta\bar{z}$, the difference between \bar{z}^+ and \bar{z}^- . This is because that the energy stored in the EDLC during the charging induces the rearrangement of the electrolyte, and the amount can be quantified with $\delta\bar{z}$. $\delta\bar{z}$ is a scalar quantity which can be simply calculated by averaging the perpendicular displacement of ions without considering a complex ionic layer structure. In other words, we can calculate how much each ionic species contributes to the stored charge in EDLC by calculating their perpendicular displacements. As described in Fig. 8, about 75% of charge stored on the electrode is induced by the rearrangement of $[SCN]^-$ ions, which is consistent with the observation that the differential capacitance of the EDLC is dominated by desorption of the anion.

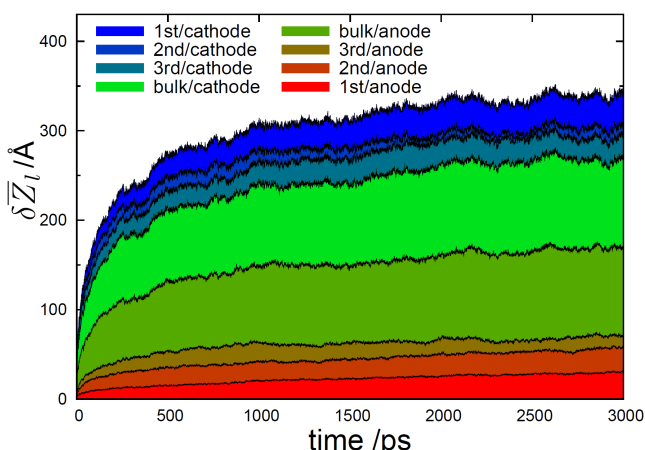


Fig. 9 $\delta\bar{Z}_l(\Delta t)$ of each ionic layer when EDLC is charged with $\Delta\Psi = 3$ V. $\delta\bar{Z}_l$ value of each layer is depicted as the colored area.

Based on the fact that the electrode charge is consistent with the perpendicular displacement of ions, we can calculate how each ionic layer contributes to the electrode charge. Ions are distinguished according to the distance from the electrode at the beginning of the charging simulations. As mentioned for $n_\alpha(z)$, at $\Delta\Psi = 0$ V, the ionic layers of $[\text{EMIM}]^+$ and $[\text{SCN}]^-$ ions are positioned at the same location because of their parallel alignment to the electrode. Thus, the three ionic layers from the electrode surface are classified through the boundary at which $n_{[\text{SCN}]}(z)$ is minimum. As depicted by the black vertical lines in Fig. 3, the ions located at $\Delta z = 0 \sim 5.9$, $5.9 \sim 9.5$, $9.5 \sim 13.7$ Å are defined as the 1st, 2nd and 3rd ionic layers, respectively. The ions 13.7 Å or more away from the electrode are defined as bulk ions. It has been checked that our discussion does not alter qualitatively even if the boundary values change slightly.

The total perpendicular displacement of the l th ionic layer of the ion α , \bar{Z}_l^α , is defined as

$$\bar{Z}_l^\alpha(\Delta t) = \sum_{i=1}^{N_l^\alpha} [z_i^\alpha(t = \Delta t) - z_i^\alpha(t = 0)], \quad (9)$$

where $\{i | z_i^\alpha(t = 0) \in l\text{th layer}\}$.

Here, N_l^α is the number of α ions in the l th layer at time $t = 0$. Therefore, \bar{Z}_l^α represents the sum of the perpendicular displacement of α ions belonging to the l th layer at time $t = 0$. In addition, $\delta\bar{Z}_l$ is defined as following equation,

$$\delta\bar{Z}_l = \bar{Z}_l^+ - \bar{Z}_l^-. \quad (10)$$

Similar to $\delta\bar{z}$, $\delta\bar{Z}_l$ can be interpreted as a contribution of the l th ionic layer to the charge stored in the EDLC. The time evolution of $\delta\bar{Z}_l$ when EDLC is charging under $\Delta\Psi = 3$ V condition is depicted in Fig. 9. $\delta\bar{Z}_l$ at different potential conditions are also shown in Fig. S6 in the supplementary information. Even though the applied potential is different, the evolution of the $\delta\bar{Z}_l$ is not significantly affected. In addition, the ionic displacement occurs not only in a particular layer but also in all ionic layers.

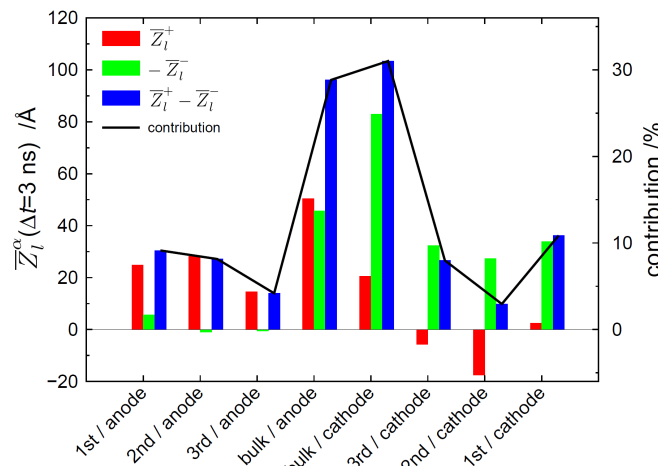


Fig. 10 The histogram of the total displacement of the l th ionic layer under charging at $\Delta\Psi = 3$ V. The blue bar denotes $\bar{Z}_l^\alpha(\Delta t = 3 \text{ ns})$ of each layer, which can be interpreted as the electrode charge contribution of the corresponding layer, as depicted by the black line. Red and green bars represent $\bar{Z}_l^+(\Delta t = 3 \text{ ns})$ and $\bar{Z}_l^-(\Delta t = 3 \text{ ns})$, respectively.

The contribution of each layer to the electrode charge is compared through $\delta\bar{Z}_l$ at $\Delta t = 3$ ns, within which the charging process is complete. Fig. 10 shows the corresponding contribution of all ionic layers and their constituent ions. The histogram summarizes our findings. (1) In the vicinity of the electrode, the contribution of the co-ion of the electrode is greater than that of the counter-ion. Due to the geometric interaction of the electrodes, the counter-ions in the first ionic layer can no longer get close to the electrodes, but the co-ions can easily fall into the bulk area. This vacating effect expected to be common in the EDLC consisting of ionic liquid electrolytes and planar electrodes. (2) The contribution of the bulk ions is more than half of the entire system. The important role of bulk ions in the EDLC is in contrast to the conventional idea that the electric double layer within a subnanometer scale completely screens the electrode charges. The conventional electric double layer concept should be used with great caution in the ionic liquid EDLCs. (3) The total contribution of the anion is greater than that of the cation, which indicates that the charging contribution of each ion species need not be the same. $[\text{EMIM}]^+$ ion is slower than $[\text{SCN}]^-$ ion due to its larger size and heavy molecular weight. Combining these results, we find out that the rearrangement of the ion itself plays an important role in charging of the ionic liquid-based EDLC. Thus, when designing the EDLC with good performance, it is necessary to consider the properties of bulk ionic liquids, especially the ion mobility.

3.5 Discharging dynamics

As with the charging process of the EDLC, we also examined the discharging dynamics by switching the electrode potential $\Delta\Psi$ from finite values to zero. Fig. 11 (a) compares the electrode charge during charging and discharging processes. Similar to the charging process, discharging of the EDLC shows fast dynamics; most of the electrode charges relax within 2 ns. In order to extract

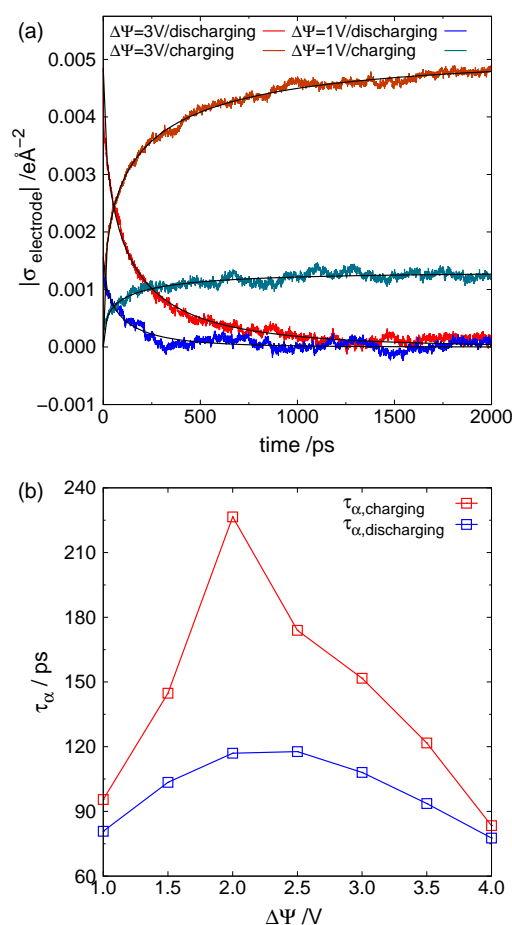


Fig. 11 (a) The charge density of the electrode when charging/discharging. Black solid lines are fitted curves with the stretched exponential function. (b) The charging/discharging time of the EDLC as a function of $\Delta\Psi$. Blue and red lines respectively denote the τ_α of discharging and charging processes.

the timescale of the discharging processes, the electrode charges are fitted with the stretched exponential function as follows,

$$\sigma(t) = \sigma_{t=0} \exp(-(t/\tau_\alpha)^\beta), \quad (11)$$

where τ_α and β are fitting parameters. The relaxation times of the discharging processes from several potential conditions are depicted in the Fig. 11 (b). The discharging time is slightly shorter than the charging times at overall potential conditions. In a discharged state, cations and anions are adjacent to each other to maximize the stability of the Coulomb interaction. On the other hand, cations and anions form alternating layers in a charged state, as depicted in Fig. 3. Therefore, the discharging process exhibits faster dynamics than charging because the ions in the initial state experiences the repulsive force with the adjacent co-ions.

The discharging and charging dynamics of the EDLC in our system are almost symmetric. Even though the discharging dynamics is faster than the charging dynamics, the order of the timescales are the same. In addition, the discharging dynamics also exhibits

the slowest when the EDLC is discharging from the $\Delta\Psi = 2\text{ V}$ condition, similar to the charging dynamics. The (dis)charging of the EDLC is induced by the rearrangement of the ionic layers, and ions near a flat electrode can rearrange their structure without a severe constraint, so the charging and discharging mechanisms are not significantly different from each other. That is, the discharging process can be understood as an inverse process of the charging process. However, a recent charging simulation in the nanoporous electrode revealed that charging and discharging dynamics are asymmetric.⁶⁸ The charging of ionic liquids in the sub-nanoporous electrode occurs with an initial condensation of the total ion density followed by the co-ion expulsion, but discharging is induced by the ion swapping. This result implies that the steric constraint of the ions near the electrode can change the charging mechanism of the EDLC. Therefore, it is necessary to study the charging mechanism for a variety of different electrode structures in the future.

3.6 Experimental relevance

The formation of the EDL in our system shows remarkably fast dynamics with a timescale of 1 ns. The charging and discharging processes of the ionic liquid EDLC are not induced by the diffusion of specific ions but a rearrangement of the overall ionic structure. During the rearrangement of the ionic layer, the average perpendicular displacement of each ion is within 1 Å, which is shorter than the size of the ion itself. Therefore, the EDL of ionic liquids can be rapidly formed by the rotation of ions or the cooperative motion with the adjacent ions without translation over long distances. The fast charging dynamics of the ionic liquid EDL suggests the possibility of the EDLC with high power density. However, the EDLC of the ionic liquid implemented in experiments does not show a fast charging dynamics as suggested in our study.²⁹ In our study, the distance between the electrodes is three to four times smaller than in typical experiments, and this may lead to a significantly faster dynamics of the EDLC. Therefore, the timescale calculated in our study can be regarded as a lower limit of the charging times of the EDLC.

Another reason for the gap between our findings and other experimental results is the electrode structure. In typical EDLC experiments, nanoporous electrodes are used to increase the energy density,² but the electrode in our system has a simple flat geometry. Recent studies revealed that the ruggedness and the curvature of the electrode may affect the differential capacitance of the EDLC.^{8,69} In addition, the transfer of ions becomes slower under nanoconfinement condition,^{70,71} which indicates that the power density of the ionic liquid EDLC can be reduced by the nanoporous electrode geometry. Nevertheless, recent studies have shown that ionic liquids in nanopores are not always slower, rather they may exhibit faster dynamics within nanopores of optimal sizes.^{72,73} Thus, if nanopores of the electrode are well designed for ionic liquids, it is expected to realize the ionic liquid EDLC with high charging rates as described in our study.

4 Conclusion

In summary, the structure and charging dynamics of an EDLC system, consisting of graphene and $[\text{EMIM}]^+[\text{SCN}]^-$, were studied using both equilibrium and non-equilibrium MD simulations. To describe the dynamics of the system accurately, the fluctuation of the electrode charge was considered by applying the constant potential simulation. It was confirmed that the correlation between the electrode charge and the adjacent ion is important in the ionic liquid-based EDLC. The ionic layer was described in terms of the orientation of the constituent ions as well as the distance from the electrodes. In the discharged state, both $[\text{EMIM}]^+$ and $[\text{SCN}]^-$ ions formed layer structures parallel to the electrodes, and the layer with such a directionality was maintained over three layers. If the electrode is charged, the ions near the electrode do not merely translate, but perform rotational motions as well, so that the ionic layers are completely rearranged. The rearrangement of the ion layer is not limited to the electrode surface but occurs over a long range scale.

The non-equilibrium charging simulations in the present study provided the molecular insight to understand the charging mechanism of the EDLC with ionic liquid electrolytes. The charging process shows a multiple time scale dynamics across the time scale corresponding to the diffusive motion of the ion and the rearrangement of the ionic layers, so the charging of the EDLC follows the heterogeneous dynamics. Especially, the charge accumulated on the electrodes during the charging process can be quantified by the perpendicular displacement of the ions. From the displacement of ions, the contribution of each ion to the electrode charge was directly calculated. In the electric double layer adjacent to the parallel electrode, the desorption of the co-ion is more pronounced than the counter-ion adsorption, which is named vacating effect. In addition, the interfacial ionic layer alone cannot completely screen the electrode charge, so bulk state ions play an important role in the electrical performance of the EDLC. The formation of the electric double layer is induced by the collective motion of overall ions. Therefore, the displacement of each ion during the charging process is shorter than its ion size, and the EDLC shows a remarkably fast charging dynamics.

We conclude by providing our rationale that the non-equilibrium charging dynamics of the EDLC can reveal the behavior of the differential capacitance of the EDLC. Our study revealed that the differential capacitance of the EDLC and its ionic layer structure are closely related to each other. The vacating effect and the ion exchange between ionic layers, which are identified as key phenomena in determining the behavior of differential capacitance, were revealed through the non-equilibrium charging study. In addition, the non-equilibrium simulation has the advantage of directly observing the motion of ions according to the potential difference changes, which is impossible in equilibrium studies. In particular, a strong correlation between the slowest charging dynamics and the maximum differential capacitance suggests that the differential capacitance of the EDLC can be predicted by non-equilibrium charging dynamics of the EDLC. It is worthwhile to pursue the quantitative relation between the charging dynamics and the complex shape of the differential capacitance of the EDLC

for various ionic liquids in the future.

Conflicts of interest

There are no conflicts to declare.

Acknowledgements

This research was supported by Creative Materials Discovery Program through the National Research Foundation of Korea (NRF) funded by the Ministry of Science, ICT and Future Planning (NRF-2017M3D1A1039553)

Notes and references

- 1 R. Burt, G. Birkett and X. S. Zhao, *Phys Chem Chem Phys*, 2014, **16**, 6519–6538.
- 2 A. González, E. Goikolea, J. A. Barrena and R. Mysyk, *Renewable and Sustainable Energy Reviews*, 2016, **58**, 1189 – 1206.
- 3 S. W. Park, A. D. DeYoung, N. R. Dhumal, Y. Shim, H. J. Kim and Y. Jung, *J Phys Chem Lett*, 2016, **7**, 1180–1186.
- 4 M. M. Islam, M. T. Alam, T. Okajima and T. Ohsaka, *Journal of Physical Chemistry C*, 2009, **113**, 3386–3389.
- 5 X. H. Liu, Y. Y. Wang, S. Li and T. Y. Yan, *Electrochimica Acta*, 2015, **184**, 164–170.
- 6 A. A. Kornyshev, *Journal of Physical Chemistry B*, 2007, **111**, 5545–5557.
- 7 G. Feng, J. Huang, B. G. Sumpter, V. Meunier and R. Qiao, *Phys Chem Chem Phys*, 2011, **13**, 14723–14734.
- 8 Z. Z. Hu, J. Vatamanu, O. Borodin and D. Bedrov, *Electrochimica Acta*, 2014, **145**, 40–52.
- 9 J. Vatamanu, M. Vatamanu, O. Borodin and D. Bedrov, *J Phys Condens Matter*, 2016, **28**, 464002.
- 10 Y. Lauw, M. D. Horne, T. Rodopoulos, A. Nelson and F. A. M. Leermakers, *Journal of Physical Chemistry B*, 2010, **114**, 11149–11154.
- 11 Y. Shim, H. J. Kim and Y. Jung, *Faraday Discuss.*, 2012, **154**, 249–263.
- 12 Y. Shim, Y. Jung and H. J. Kim, *The Journal of Physical Chemistry C*, 2011, **115**, 23574–23583.
- 13 J. Vatamanu and D. Bedrov, *The Journal of Physical Chemistry Letters*, 2015, **6**, 3594–3609.
- 14 M. V. Fedorov and A. A. Kornyshev, *Chemical Reviews*, 2014, **114**, 2978–3036.
- 15 J. Chmiola, G. Yushin, Y. Gogotsi, C. Portet, P. Simon and P. L. Taberna, *Science*, 2006, **313**, 1760–1763.
- 16 S. Kondrat, C. Kornyshev, V. Pérez, Y. Presser and A. Gogotsi, *Energy and Environmental Science*, 2012, **5**, 6474–6479.
- 17 D. A. Brownson, D. K. Kampouris and C. E. Banks, *Journal of Power Sources*, 2011, **196**, 4873–4885.
- 18 X. Huang, Z. Zeng, Z. Fan, J. Liu and H. Zhang, *Advanced Materials*, 2012, **24**, 5979–6004.
- 19 Y. Chen, X. Zhang, D. Zhang, P. Yu and Y. Ma, *Carbon*, 2011, **49**, 573–580.
- 20 W.-Y. Tsai, R. Lin, S. Murali, L. Li Zhang, J. K. McDonough, R. S. Ruoff, P.-L. Taberna, Y. Gogotsi and P. Simon, *Nano Energy*, 2012, **2**, 403–411.

- 21 S. Jo, S.-W. Park, Y. Shim and Y. Jung, *Electrochimica Acta*, 2017, **247**, 634–645.
- 22 S. Jo, S.-W. Park, C. Noh and Y. Jung, *Electrochimica Acta*, 2018, **284**, 577–586.
- 23 A. D. DeYoung, S. W. Park, N. R. Dhumal, Y. Shim, Y. Jung and H. J. Kim, *Journal of Physical Chemistry C*, 2014, **118**, 18472–18480.
- 24 S. M. Mahurin, S. P. Surwade, M. Crespo and S. Dai, *Journal of Raman Spectroscopy*, 2016, **47**, 585–590.
- 25 R. Thangavel, A. G. Kannan, R. Ponraj, V. Thangavel, D.-W. Kim and Y.-S. Lee, *Journal of Power Sources*, 2018, **383**, 102–109.
- 26 V. Lockett, M. Horne, R. Sedev, T. Rodopoulos and J. Ralston, *Phys Chem Chem Phys*, 2010, **12**, 12499–12512.
- 27 V. Lockett, R. Sedev, J. Ralston, M. Horne and T. Rodopoulos, *Journal of Physical Chemistry C*, 2008, **112**, 7486–7495.
- 28 G.-H. Sun, K.-X. Li and C.-G. Sun, *Journal of Power Sources*, 2006, **162**, 1444–1450.
- 29 C. Zhong, Y. Deng, W. Hu, J. Qiao, L. Zhang and J. Zhang, *Chemical Society Reviews*, 2015, **44**, 7484–7539.
- 30 H. Helmholtz, *Annalen der Physik*, 1879, **243**, 337–382.
- 31 M. Brown, Z. Abbas, A. Kleibert, R. Green, A. Goel, S. May and T. Squires, *Physical Review X*, 2016, **6**, 011007.
- 32 M. Z. Bazant, B. D. Storey and A. A. Kornyshev, *Phys Rev Lett*, 2011, **106**, 046102.
- 33 Z. A. Goodwin, G. Feng and A. A. Kornyshev, *Electrochimica Acta*, 2017, **225**, 190–197.
- 34 D. T. Limmer, *Phys. Rev. Lett.*, 2015, **115**, 256102.
- 35 J. M. Griffin, A. C. Forse, W.-Y. Tsai, P.-L. Taberna, P. Simon and C. P. Grey, *Nature Materials*, 2015, **14**, 812–820.
- 36 M. Mezger, H. Schröder, H. Reichert, S. Schramm, J. S. Okasinski, S. Schöder, V. Honkimäki, M. Deutsch, B. M. Ocko, J. Ralston, M. Rohwerder, M. Stratmann and H. Dosch, *Science*, 2008, **322**, 424–428.
- 37 M. Mezger, S. Schramm, H. Schröder, H. Reichert, M. Deutsch, E. J. De Souza, J. S. Okasinski, B. M. Ocko, V. Honkimäki and H. Dosch, *The Journal of Chemical Physics*, 2009, **131**, 094701.
- 38 J. M. Black, D. Walters, A. Labuda, G. Feng, P. C. Hillesheim, S. Dai, P. T. Cummings, S. V. Kalinin, R. Proksch and N. Balke, *Nano Letters*, 2013, **13**, 5954–5960.
- 39 L. A. Jurado and R. M. Espinosa-Marzal, *Scientific Reports*, 2017, **7**, 4225.
- 40 K. Kirchner, T. Kirchner, V. Ivaniščev and M. Fedorov, *Electrochimica Acta*, 2013, **110**, 762–771.
- 41 J. Vatamanu, O. Borodin, D. Bedrov and G. D. Smith, *The Journal of Physical Chemistry C*, 2012, **116**, 7940–7951.
- 42 M. V. Fedorov and A. A. Kornyshev, *Electrochimica Acta*, 2008, **53**, 6835–6840.
- 43 M. V. Fedorov, N. Georgi and A. A. Kornyshev, *Electrochemistry Communications*, 2010, **12**, 296–299.
- 44 D. T. Limmer, M. Salanne, R. van Roij, P. A. Madden, D. Chandler and B. Rotenberg, *The Journal of Physical Chemistry C*, 2014, **118**, 18291–18298.
- 45 K. Xu, X. Ji, B. Zhang, C. Chen, Y. Ruan, L. Miao and J. Jiang, *Electrochimica Acta*, 2016, **196**, 75–83.
- 46 X. Jiang, J. Huang, H. Zhao, B. G. Sumpter and R. Qiao, *Journal of Physics: Condensed Matter*, 2014, **26**, 284109.
- 47 X. Kong, D. Lu, Z. Liu and J. Wu, *Nano Research*, 2015, **8**, 931–940.
- 48 C. Péan, C. Merlet, B. Rotenberg, P. A. Madden, P.-L. Taberna, B. Daffos, M. Salanne and P. Simon, *ACS Nano*, 2014, **8**, 1576–1583.
- 49 F. Endres, D. MacFarlane and A. Abbott., *Electrodeposition from ionic liquids*, Wiley-VCH, Weinheim, 2008, p. 26.
- 50 J. N. Canongia Lopes, J. Deschamps and A. A. H. Pádua, *The Journal of Physical Chemistry B*, 2004, **108**, 2038–2047.
- 51 J. N. Canongia Lopes, J. Deschamps and A. A. H. Pádua, *The Journal of Physical Chemistry B*, 2004, **108**, 11250–11250.
- 52 K. B. Dhungana, L. F. O. Faria, B. Wu, M. Liang, M. C. C. Ribeiro, C. J. Margulis and E. W. Castner, *The Journal of Chemical Physics*, 2016, **145**, 024503.
- 53 G. Hummer, J. C. Rasaiah and J. P. Noworyta, *Nature*, 2001, **414**, 188–190.
- 54 S. Plimpton, *Journal of Computational Physics*, 1995, **117**, 1–19.
- 55 S. K. Reed, O. J. Lanning and P. A. Madden, *The Journal of Chemical Physics*, 2007, **126**, 084704.
- 56 Z. Wang, Y. Yang, D. L. Olmsted, M. Asta and B. B. Laird, *The Journal of Chemical Physics*, 2014, **141**, 184102.
- 57 I.-C. Yeh and M. L. Berkowitz, *The Journal of Chemical Physics*, 1999, **111**, 3155–3162.
- 58 R. W. Hockney, *Computer simulation using particles / R.W. Hockney and J.W. Eastwood.*, Taylor & Francis, Special student ed.. edn, 1988.
- 59 J. Vatamanu, O. Borodin and G. D. Smith, *Journal of the American Chemical Society*, 2010, **132**, 14825–14833.
- 60 G. Feng, J. S. Zhang and R. Qiao, *Journal of Physical Chemistry C*, 2009, **113**, 4549–4559.
- 61 C. Merlet, M. Salanne, B. Rotenberg and P. A. Madden, *The Journal of Physical Chemistry C*, 2011, **115**, 16613–16618.
- 62 S. Tazi, M. Salanne, C. Simon, P. Tury, M. Pounds and P. A. Madden, *Journal of Physical Chemistry B*, 2010, **114**, 8453–8459.
- 63 S.-W. Park, *PhD thesis*, Seoul National University, Seoul, Korea, 2016.
- 64 S.-W. Park, S. Kim and Y. Jung, *Phys. Chem. Chem. Phys.*, 2015, **17**, 29281–29292.
- 65 S. Kim, S.-W. Park and Y. Jung, *Phys. Chem. Chem. Phys.*, 2016, **18**, 6486–6497.
- 66 D. Kim, D. Jeong and Y. Jung, *Phys. Chem. Chem. Phys.*, 2014, **16**, 19712–19719.
- 67 P. Reichert, K. S. Kjær, T. Brandt van Driel, J. Mars, J. W. Ochsmann, D. Pontoni, M. Deutsch, M. M. Nielsen and M. Mezger, *Faraday Discuss.*, 2018, **206**, 141–157.
- 68 J. Vatamanu, O. Borodin, M. Olguin, G. Yushin and D. Bedrov, *Journal of Materials Chemistry A*, 2017, **5**, 21049–21076.
- 69 K. Ma, C. E. Woodward and J. Forsman, *The Journal of Physi-*

- cal Chemistry C, 2014, **118**, 15825–15834.
- 70 S. Perkin, *Phys. Chem. Chem. Phys.*, 2012, **14**, 5052–5062.
- 71 J. Monk, R. Singh and F. R. Hung, *The Journal of Physical Chemistry C*, 2011, **115**, 3034–3042.
- 72 C. Iacob, J. R. Sangoro, W. K. Kipnusu, R. Valiullin, J. Kärger and F. Kremer, *Soft Matter*, 2012, **8**, 289–293.
- 73 Y. He, R. Qiao, J. Vatamanu, O. Borodin, D. Bedrov, J. Huang and B. G. Sumpter, *The Journal of Physical Chemistry Letters*, 2016, **7**, 36–42.